

Structural, Electrical, and Magnetic Properties of α-$(ET)_7[MnCl_4]_2 \cdot (1,1,2\text{-}C_2H_3Cl_3)_2$ (ET = Bis(ethylenedithio)tetrathiafulvalene)

Toshio Naito,[*,1,2,3] **and Tamotsu Inabe**[2]

[1]Creative Research Initiative "Sousei" (CRIS), Hokkaido University, Kita 21, Nishi 10, Kita-ku, Sapporo 001-0021

[2]Division of Chemistry, Graduate School of Science, Hokkaido University, Sapporo 060-0810

[3]Institute for Molecular Science, Nishigonaka 38, Myodaiji-cho, Okazaki 444-8585

Received March 23, 2004; E-mail: tnaito@sci.hokudai.ac.jp

A new charge-transfer salt of ET with a chloromanganate(II) complex anion has been synthesized and characterized by X-ray structural analysis, resistivity measurements, magnetic susceptibility, electron spin resonance (ESR), and an extended Hückel tight biding (EHTB) band calculation. The crystal has a sheet structure comprised of an α-type two-dimensional (2D) donor arrangement in the *bc*-plane and insulating sheets of discrete $[MnCl_4]^{2-}$ anions and 1,1,2-$C_2H_3Cl_3$ (TCE) molecules. Its conducting property exhibits considerable anisotropy, which is of effectively metallic along the *b*-axis down to 1.2 K under 2.9 kbar and higher pressure. The magnetic susceptibility is approximately reproduced by the Curie–Weiss law with a Weiss temperature of $\theta = -(1.35 \pm 0.07)$ K from 2–300 K. ESR measurements revealed that the π-electron system in this salt exhibits Pauli paramagnetism at least at 3.6 to ~50 K. The band calculation suggests that the HOMO (the highest occupied molecular orbital) band has very small dispersion, almost solely along the b^*-axis.

In the research field of molecular materials, the charge-transfer (CT) salts of chalcogen-donor molecules containing magnetic transition metal complex anions have attracted worldwide interest for quite some time,[1–7] mainly because new phenomena can be expected from the coexistence of conduction and localized electronic systems. In addition, in ET salts, the chloromanganates have shown their rich chemistry by presenting a wide variety of shapes and charges of metal complexes.[8–13] Accordingly, the resultant crystal structures and physical properties vary from salt to salt, which has been encouraging researchers to carry out the synthesis and characterization of related salts. Here, we report on a new example α-$(ET)_7(MnCl_4)_2(1,1,2\text{-}C_2H_3Cl_3)_2$, which is interesting from the following points of view. Firstly, a tight-binding calculation suggests that it should have a very narrow HOMO band. This could result in an enhancement of the effective mass of the conduction electrons when the system is a metal; unusual physical properties often occur in such electronic systems. Secondly, this salt exhibits a stable metallic property, which is exceptional for one-dimensional (1D) conductors. In this paper we will discuss the title compound (α-salt), while comparing it with a structurally related salt, β''-$(ET)_3(MnCl_4)(TCE)$ (β''-salt).[10]

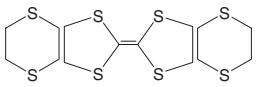

ET

Scheme 1.

Experimental

Materials. ET was purchased from Tokyo Chemical Industry Co., Ltd. and used as received. Single crystals were obtained by similar electrochemical crystallizations as described before.[10] Typically, ET (18–20 mg), $[Mn_{12}O_{12}(C_6H_5COO)_{16}(H_2O)_4]$[14] (3–4 mg), and $(C_6H_5)_4P[Mn_{12}O_{12}(C_6H_5COO)_{16}(H_2O)_4]$[15,16] (35–55 mg) were added to distilled 1,1,2-$C_2H_3Cl_3$ (50 mL) containing 8–10% (vol/vol) C_2H_5OH in a nitrogen atmosphere, and the solutes were dissolved at room temperature (RT) as much as possible with an ultrasonic device. The resultant dark-brown mixture was left standing overnight and electrolyzed with platinum electrodes (1 mmϕ wires) and a constant current of 2.5 μA at 20 °C for 2–3 weeks. The electrolytic cells used were equipped with glass frits of fine porosity (G2) and a Teflon three-way valve. The obtained crystals were shiny black rhomboid thick plates with typical dimensions of $2 \times 1 \times 0.2$ mm.

X-ray Structural Analysis. Data collection for the title compound was carried out with a Rigaku R-AXIS RAPID Imaging Plate area detector with graphite-monochromated Mo Kα radiation ($\lambda = 0.7107$ Å) at 103 K. The intensities were collected for Lorentz and polarization effects. An empirical absorption correction was applied. The structure was solved by a direct method (SIR92),[17] and the hydrogen atoms were placed at the calculated ideal positions. A full-matrix least-squares technique on F with anisotropic thermal parameters for non-hydrogen atoms and isotropic ones for hydrogen atoms was employed for a structure refinement. Hydrogen atoms were included, but not refined. Atom scattering factors were taken from the literature.[18] The values for the mass attenuation coefficients were those of Creagh and Hubbell.[19] All calculations and a part of the molecular graphics were performed using the teXsan[20] crystallographic software package from Molecular Structure Corporation; some structural

Published on the web November 11, 2004; DOI 10.1246/bcsj.77.1987

Table 1. Parameters Set for the EHTB Calculation

Elements	Atomic orbital	H_{ii}/eV[a)]	Zeta1	Coefficient1	Zeta2	Coefficient2
S	s	−20.0	2.662	0.5564	1.688	0.4873
S	p	−13.3	2.238	0.5212	1.333	0.5443
C	s	−21.4	1.831	0.7616	1.153	0.2630
C	p	−11.4	2.730	0.2595	1.257	0.8025
H	s	−13.6	1.300	1.00		

a) Valence state ionization potential.

views were produced using Ortep3 for Windows.[21] The final values of the refined atomic parameters with esd's, bond distances and angles together with other details of the experimental conditions are deposited in a CIF file as Supporting Information. Crystallographic data have been deposited at the CCDC, 12 Union Road, Cambridge CB2 1EZ, UK and copies can be obtained on request, free of charge, by quoting the publication citation and the deposition number CCDC-245981.

Calculations of Overlap Integrals and Band Structures. The band calculation was carried out based on the EHTB method using a commercially available program package, CAESAR.[22] In calculating the off-diagonal matrix elements, $H_{ij} = \langle \chi_i | H^{\text{eff}} | \chi_j \rangle$, the weighted formula was used.[23] The valence atomic orbitals were approximated by double-zeta Slater-type orbitals. The actual atomic orbital parameters used for the EHTB calculation are tabulated in Table 1.

Measurements. All of the measurements were carried out immediately after the filtration of single crystals, which were quickly identified to be the desired product of sufficiently good quality by X-ray photographs using a Rigaku Imaging Plate. Because the sample includes the solvent molecules in the crystal, we considered the possibility of decomposition of the lattice by a loss of the solvent molecules during the measurements. After measuring the physical properties, the sample crystals were again checked by X-ray photographs to confirm there was no significant deterioration. The details of the measurements of the electrical properties, magnetic susceptibility, and ESR spectra were previously described.[10]

Electrical Properties. The electrical resistivity was measured (RT–1.2 K; 0–14.8 kbar) using a standard direct-current 4-probe method with gold wires (20 μmϕ) and gold paints (Tokuriki Chemical Research Co., Ltd., No. 8560), and a Be/Cu clump-type cell on high-pressure measurements. The pressure medium used was Daphne oil 7373 (Idemitsu Co., Ltd.). The applied pressure values were measured at RT, and not corrected for solidification and thermal contraction of the pressure medium at low temperature. The current was applied on the most-developed facet (*bc*-plane) of the single crystals. The linearity between the applied current and the observed voltage in a sample was checked at the every start of the measurements.

Magnetic Susceptibility. A few mg of single crystals (ca. 20–30 in number) were selected and set in a SQUID (Superconducting Quantum Interference Device) susceptometer (MPMS-5S of Quantum Design) with a field strength of 0.8 T. The linearity of magnetization up to 5.0 T was checked at 5 K by measuring the magnetization curve. The examined temperature range was 2–300 K and the diamagnetic correction was carried out using the observed value for an ET molecule and by the Pascal law for the other species.

ESR Spectra. The ESR spectra of the X-band (9.3 GHz) were measured on the single crystal in the temperature range of 3.6–300 K using an EMX EPR Spectrometer (Bruker) equipped with a continuous-flow cryostat, ESR 900 (Oxford). The temperature was controlled so as not to allow the temperature variation to exceed ±0.5 K or ±1% of the set value during a field sweep. An rhomboid–plate-shaped crystal was mounted on a Teflon rod, settled with a minimum amount of grease (Apiezon N), and sealed in a 5 mm-diameter quartz tube in a helium atmosphere of ca. 20 Torr. The Teflon rod was also settled at the bottom of the quartz tube with a minimum amount of the same grease. The quartz tube was equipped with a circular protractor, and the anisotropy of the spectra was examined within ±1° accuracy by rotating the quartz

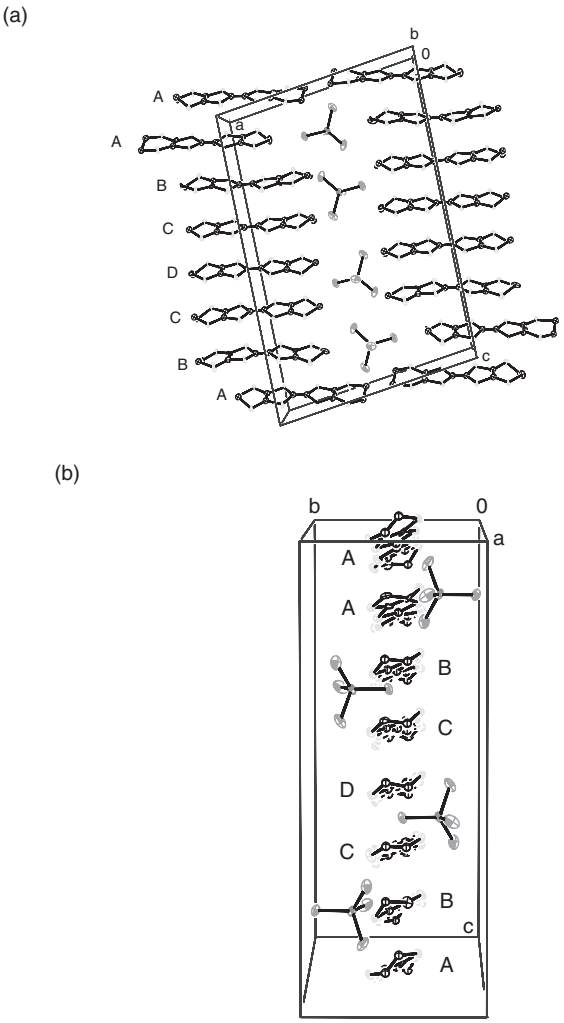

Fig. 1. Unit cell; front view of (a) *ac*-, and (b) *bc*-planes. Hydrogen atoms are omitted for clarity.

tube about the long axis of the specimen, which nearly coincided with the [001]-direction. Magnetic fields were applied parallel and perpendicular to the conductive direction, i.e., the *b*-axis of the single crystal. These directions of the magnetic fields are designated by the 0- and 90-direction, respectively below. The measurement was carried out on several samples under different conditions, and the signal was checked not to be saturated at 3.6 K, 70 K, and 297 K during every measurement.

Results and Discussion

Crystal and Band Structures. Figures 1 and 2 show the molecular and crystal structures of α-$(ET)_7(MnCl_4)_2(1,1,2\text{-}C_2H_3Cl_3)_2$. The crystal structure was confirmed to be retained from RT–103 K. Here, we discuss the structure based on the data taken at 103 K. A crystallographic data summary is given in Table 2. Selected bond distances and angles are given in Tables 3 and 4. The asymmetric unit contains three and a half ET molecules (A, B, C, D), one $[MnCl_4]$ anion and one 1,1,2-$C_2H_3Cl_3$ (TCE) molecule. The $[MnCl_4]$ anion is an almost ideally regular tetrahedral with Mn–Cl bond distances of 2.3–2.4 Å. Accordingly, the oxidation state of the Mn atom is considered to be +2, which is consistent with prior work.[8,10,24] The ET molecules stack along the *c*-axis to make a columnar structure with a 7-fold period (A, B, C, D, C, B, A). Viewing the ET

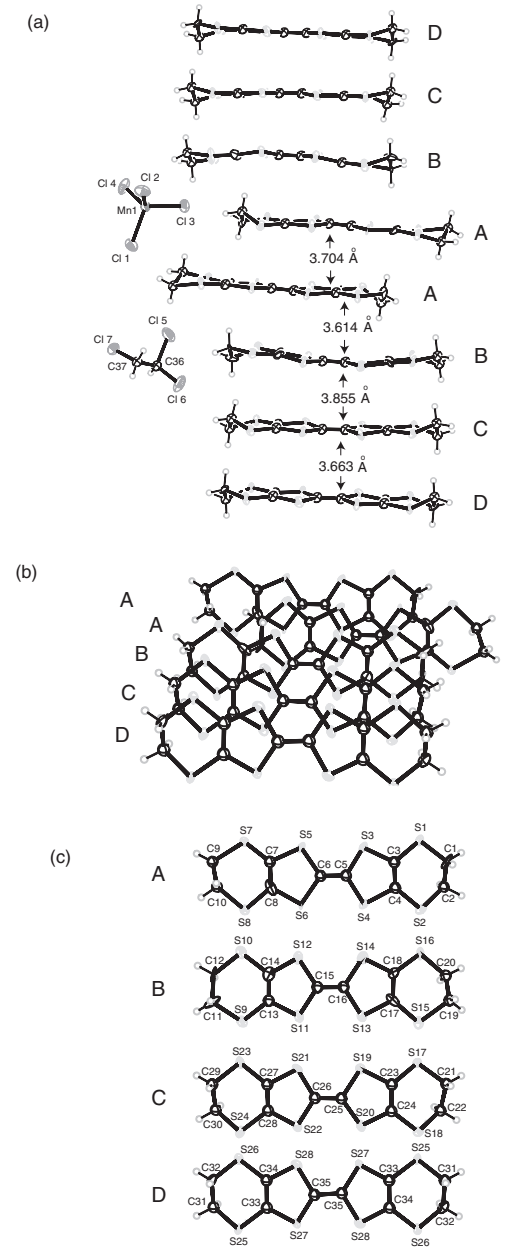

Fig. 2. Molecular arrangement of the ET stack. (a) side-view, (b) top-view, and (c) each molecular structure and atomic numbering scheme of the crystallographically independent ET molecules.

Table 2. Crystallographic Data Summary of the Title Salt

Chemical formula	$C_{74}H_{62}S_{56}Cl_{14}Mn_2$
Formula weight	3352.88
Crystal habit	Black platelet
Crystal dimensions/mm	$0.50 \times 0.13 \times 0.03$
Crystal system	Monoclinic
Space group	$P2_1/c$ (#14)
a/Å	18.8959(6)
b/Å	11.2945(3)
c/Å	28.770(1)
β/°	97.599(1)
V/Å^3	6086.1(3)
Z	2
D_{calcd}/g cm^{-3}	1.829
μ(Mo Kα)/cm^{-1}	15.18
F_{000}	3380.00
Temperature/K	103
No. of reflection measured	13905
No. of independent reflections observed	1121 [$I > 3\sigma(I)$]
Maximum 2θ value/°	55
No. of variable parameters	608
Structure solution	Direct methods (SIR92)
Refinement	Full-matrix least-squares on F
Function minimized	$\Sigma w(\|F_o\| - \|F_c\|)^2$
Least squares weights	$1/\sigma^2(F_o) = 4F_o^2/\sigma^2(F_o^2)$
Anomalous dispersion	All non-hydrogen atoms
R	0.055
R_w	0.071
Goodness of fit indicator	1.23
Max shift/error in final cycle	0.39
Maximum peak in final diff. map	0.48 e$^-$ Å^{-3}
Minimum peak in final diff. map	-0.42 e$^-$ Å^{-3}

$R = \Sigma||F_o| - |F_c||/\Sigma|F_o|$, $R_w = [\Sigma w(|F_o| - |F_c|)^2/\Sigma wF_o^2]^{1/2}$.

Table 3. Selected Bond Distances (Å) of the Title Salt

Mn(1)–Cl(1)	2.35(2)	Mn(1)–Cl(2)	2.39(2)
Mn(1)–Cl(3)	2.27(2)	Mn(1)–Cl(4)	2.37(2)
C(3)–C(4)	1.32(4)	C(5)–C(6)	1.37(6)
C(7)–C(8)	1.42(5)	C(13)–C(14)	1.2(1)
C(15)–C(16)	1.22(3)	C(17)–C(18)	1.28(4)
C(23)–C(24)	1.40(6)	C(25)–C(26)	1.35(6)
C(27)–C(28)	1.31(4)	C(33)–C(34)	1.34(6)
C(35)–C(35)	1.48(5)		

column down along the stacking axis, each ET molecule is not located right above the next one, but progressively (~1.324 Å) slips aside along the short molecular axis. This is thermodynamically favorable for avoiding a steric hindrance, as well as keeping a maximal overlap between the adjacent molecular orbitals. This situation is realized by tilting the molecular planes by ca. 28° from the stacking axis. In order to stabilize the unpaired electrons in the HOMOs of ET by delocalizing them among the neighboring molecules, one choice is to make the tilt angle alternate from one column to the next one (+28°, −28°, +28°, ...) since this enables the closest packing as well as maximal overlap between the HOMOs of ET molecules on the neighboring columns. As a result, the columns are closely gathered to make a 2D sheet in the *bc*-plane. Such a donor molecular arrangement is called α-type.[25] This sheet alternates with an insulating sheet containing the $[MnCl_4]^{2-}$ anion and the TCE molecule along the *a*-axis. The TCE molecules face the ET molecules of A and B, while the $[MnCl_4]^{2-}$ anions are located in the spaces surrounded by the four ET molecules: (B, C, B, and C) or (A, B, C, and D). The Cl atoms on the anions and TCE molecules are inserted in the ET sheets. There are some intermolecular atomic contacts among the $[MnCl_4]^{2-}$ anion, the ET and TCE molecules (Table 5). No disorder or large temperature factors, which are often observed in solvent molecules and highly symmetrical anions in crystals, are observed in the anions or in the TCE molecules. Due to the steric

Table 4. Selected Bond Angles (°) of the Title Salt

Cl(1)–Mn(1)–Cl(2)	109.2(7)	Cl(1)–Mn(1)–Cl(3)	111.1(6)
Cl(1)–Mn(1)–Cl(4)	106.3(6)	Cl(2)–Mn(1)–Cl(3)	107.7(7)
Cl(2)–Mn(1)–Cl(4)	114.8(7)	Cl(3)–Mn(1)–Cl(4)	107.7(6)
C(1)–S(1)–C(3)	101(2)	C(2)–S(2)–C(4)	89(2)
C(3)–S(3)–C(5)	92(2)	C(4)–S(4)–C(5)	96(2)
C(6)–S(5)–C(7)	101(2)	C(6)–S(6)–C(8)	96(3)
C(7)–S(7)–C(9)	111(2)	C(8)–S(8)–C(10)	102(2)
C(11)–S(9)–C(13)	96(2)	C(12)–S(10)–C(14)	106(2)
C(13)–S(11)–C(15)	95(3)	C(14)–S(12)–C(15)	96(2)
C(16)–S(13)–C(17)	91(2)	C(16)–S(14)–C(18)	96(1)
C(17)–S(15)–C(19)	96(2)	C(18)–S(16)–C(20)	112(1)
C(21)–S(17)–C(23)	94(2)	C(22)–S(18)–C(24)	105(2)
C(23)–S(19)–C(25)	99(2)	C(24)–S(20)–C(25)	105(2)
C(26)–S(21)–C(27)	83(1)	C(26)–S(22)–C(28)	93(2)
C(27)–S(23)–C(29)	106(1)	C(28)–S(24)–C(30)	99(1)
C(31)–S(25)–C(33)	100(2)	C(32)–S(26)–C(34)	104(2)
C(33)–S(27)–C(35)	97(2)	C(34)–S(28)–C(35)	120(2)

Table 5. Selected Intermolecular Short Distances (Å) of the Title Salt

ET(A)–$MnCl_4$				ET(A)–ET(C)			
C(9)–Cl(1)	3.36(3), 3.34(4)	C(10)–Cl(1)	3.68(5), 3.78(4)	S(1)–S(17)	3.41(2)	S(1)–S(19)	3.45(2)
S(8)–Cl(1)	3.83(2)	C(2)–Cl(3)	3.61(4)	S(2)–S(18)	3.67(2)	S(2)–S(20)	3.78(2)
ET(B)–$MnCl_4$				S(3)–S(21)	3.82(2)	S(3)–S(19)	3.91(2)
C(19)–Cl(2)	3.52(7)	C(20)–Cl(2)	3.31(3)	S(4)–S(22)	3.93(2)	S(4)–S(20)	3.95(2)
S(15)–Cl(3)	3.55(2)	C(20)–Cl(4)	3.30(3)	S(5)–S(23)	3.69(2)	S(5)–S(21)	3.95(2)
S(16)–Cl(4)	3.53(2)	C(11)–Cl(4)	3.77(4)	S(6)–S(24)	3.67(2)	S(7)–S(23)	3.63(2)
ET(C)–$MnCl_4$				S(8)–S(24)	3.85(2)		
C(30)–Cl(1)	3.55(4)	C(29)–Cl(2)	3.89(2)	ET(A)–ET(D)			
C(22)–Cl(3)	3.81(4)	S(18)–Cl(3)	3.77(2)	S(1)–S(25)	3.62(2)	S(1)–S(27)	3.71(2)
ET(D)–$MnCl_4$				S(2)–S(26)	3.51(2)	S(2)–S(28)	3.61(2)
C(32)–Cl(3)	3.80(4)			S(3)–S(28)	3.97(2)	S(3)–S(19)	3.91(2)
ET(A)–TCE				S(3)–S(27)	3.99(2)	S(4)–S(28)	3.95(2)
C(1)–Cl(7)	3.72(3)	C(9)–Cl(5)	3.45(2)	S(4)–S(27)	3.98(2)	S(5)–S(26)	3.46(2)
C(10)–Cl(7)	3.87(6)	S(7)–Cl(5)	3.52(2)	S(5)–S(28)	3.88(2)	S(6)–S(25)	3.72(2)
S(8)–Cl(7)	3.44(2)			S(6)–S(27)	3.98(2)	S(7)–S(26)	3.36(2)
ET(B)–TCE				S(8)–S(25)	3.57(2)		
C(12)–Cl(5)	3.52(3)	C(12)–Cl(6)	3.77(2)	ET(B)–ET(B)			
C(19)–Cl(6)	3.49(8)	S(15)–Cl(6)	3.41(2)	S(9)–S(16)	3.81(2)	S(9)–S(14)	3.83(2)
ET(C)–TCE				S(10)–S(13)	3.42(2)	S(10)–S(15)	3.55(2)
C(22)–Cl(6)	3.57(6)	C(21)–Cl(7)	3.58(4)	S(11)–S(14)	3.66(2)	S(11)–S(12)	3.84(2)
ET(D)–TCE				S(12)–S(13)	3.56(2)		
C(31)–Cl(7)	3.72(5)	S(25)–Cl(7)	3.60(2)	ET(B)–ET(C)			
TCE–$MnCl_4$				S(9)–S(24)	3.33(2)	S(9)–S(22)	3.45(2)
Cl(6)–Cl(2)	3.63(2)	C(36)–Cl(4)	3.67(5)	S(10)–S(23)	3.35(2)	S(10)–S(21)	3.54(2)
C(37)–Cl(2)	3.57(6)	C(37)–Cl(4)	3.53(5)	S(11)–S(19)	3.92(2)	S(11)–S(22)	3.98(2)
ET(A)–ET(A)				S(12)–S(19)	3.89(2)	S(13)–S(21)	3.80(2)
S(2)–S(5)	3.82(2)	S(2)–S(6)	3.85(2)	S(13)–S(18)	3.89(2)	S(14)–S(17)	3.72(2)
S(4)–S(4)	3.90(3)			S(14)–S(21)	3.81(2)	S(14)–S(22)	3.99(2)
ET(A)–ET(B)				S(15)–S(18)	3.56(2)	S(16)–S(17)	3.46(2)
S(3)–S(12)	3.98(2)			ET(C)–ET(D)			
S(6)–S(9)	3.86(2)			S(17)–S(25)	3.97(2)	S(18)–S(26)	3.92(2)
				S(20)–S(27)	3.88(2)	S(22)–S(28)	3.91(2)

Non-bonded contacts out to 4.00 Å. The van der Waals radii are $r_C = 1.70$, $r_S = 1.85$, and $r_{Cl} = 1.80$ Å.

Table 6. Comparison of Crystal Data in the α- and the β''-Salts

	α-$(ET)_7(MnCl_4)_2(TCE)_2$	β''-$(ET)_3(MnCl_4)(TCE)$
Crystal system	Monoclinic	Monoclinic
Space group	$P2_1/c$	$P2_1/m$
a/Å	18.8959(6)	9.9182(5)
b/Å	11.2945(3)	29.591(2)
c/Å	28.770(1)	10.1652
β/°	6086.1(3)	2810.8(2)
Z	2	2
D_{calcd}/g cm^{-3}	1.829	1.753
R/R_w	0.055/0.071	0.078/0.089
T/K	103	296
No. of independent ET molecules	3.5	1.5
Reference	This work	10

interaction between the ET and the $[MnCl_4]^{2-}$ anion or the TCE molecule, the center of the A molecule clearly deviates (~3.519 Å) from the others along the long axis of the molecule.

The structural properties mentioned above resemble the β''-salt,[10] where an organic sheet comprised of a 2D array of ET molecules alternates with an insulating sheet comprised of discrete $[MnCl_4]^{2-}$ anions and TCE molecules. The α-salt has approximately a double length of the stacking axis, and thus a nearly double volume of the unit cell of the β''-salt (Table 6).

The four crystallographically independent ET molecular structures are very similar to each other, which suggests that they should carry an equal molecular charge. Some of the bond lengths of ET have been known to be very sensitive to the electrical charge.[26,27] A detailed examination of the molecular structure supports that each of the ET molecules in the α-salt should have a $+4/7$ charge. In other words, the crystal structure indicates that a charge separation between the ET molecules should not occur down to 103 K. This is consistent with the calculated energy levels of their HOMOs (A, −9.810; B, −10.608; C, −9.700; D, −9.905 eV, by the extended Hückel method) and the physical properties discussed below. Further, the spin susceptibility suggests that the metallic properties should remain down to 3.6 K. This is very unusual considering the 1D electronic structure of this salt. The distances between the neighboring mean molecular planes are 3.704 (A–A), 3.614 (A–B), 3.855 (B–C), and 3.663 Å (C–D), respectively. There are many atomic contacts between the sulfur atoms ($r_{S-S} \leq 3.70$ Å) of different ET molecules on the adjacent columns, but not in the same column (Table 5). Such an intermolecular interaction is typical of α-type ET salts.[25] In addition, atomic contacts shorter than the van der Waals distance ($r_{Cl-S} = 3.65$ Å) are found between the sulfur atoms of ET and the chlorine atoms of the $[MnCl_4]^{2-}$ anions. They, however, are all still too long distances to expect any significant magnetic interactions between the conduction electrons and the localized spins, which is discussed in a latter section. Next, we quantitatively discuss the intermolecular interactions between the ET molecules.

Figure 3 shows the calculated transfer integrals using a program developed by J. Ren et al. based on the extended Hückel method.[22] The absolute values of t1, t2, t5, and t9 are fairly

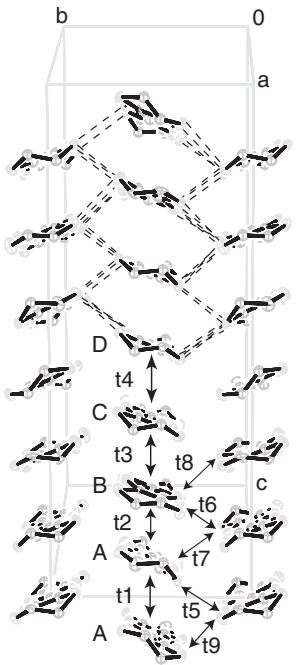

Fig. 3. Intermolecular interactions between the ET molecules (Hydrogen atoms are omitted for clarity). Broken lines indicate S–S short contacts ($r_{S-S} \leq 3.70$ Å). Arrows designated as t1 to t9 indicate calculated transfer integrals (t's) between the corresponding ET molecules. Each value (t/meV) is as follows: t1; −17.0, t2; −15.8, t3; −42.5, t4; −46.6, t5; 18.8, t6; −29.9, t7; 25.3, t8; 91.4, t9; 18.8. For simplicity and clarity of the figure, the S–S short contacts are not drawn where transfer integrals are indicated, and vice versa.

small for a conducting ET salt, which originates from the large deviation in the stack of molecule A. In addition to this irregularity of intermolecular interactions, the commensurate 7-fold periodicity of ET stacks along the c-axis is expected to open an energy gap along the c^*-direction. Thus, we carried out an EHTB band calculation using CAESAR.[22] The obtained band structure is different from those expected for stable molecular metals. Many bands coexist within a small range of energy,

and are hardly dispersive in the b^*c^*-plane (Fig. 4) with very small gaps between them. Because the Fermi level (−8.42 eV) touches on a narrow band, the system corresponds to the situation where a Fermi surface has just disappeared ("nested"). In fact, when we slightly lowered the Fermi level in the calculation, a Fermi surface appeared (not shown), which was perfectly 1D, i.e., a pair of parallel straight lines running along the c^*-direction. Generally speaking,[22] for a system with a partially filled band, a magnetic insulating state may become more stable than the metallic state due to electron–electron repulsion, when the width of the partially filled band is narrow. This is more likely especially when there is another band and the energy difference between the two bands is small enough, like in this case. These energetically close bands imply that any perturbation may cause electron hopping, presenting a metallic character at high temperature ("narrow-gap semiconductors"). On the other hand, if the bands near the Fermi level are very flat, and if there are small gaps between them, the system may be, or easily turn into, a semiconductor. Thus, the EHTB calculation suggests that this system should be a (narrow-gap) semiconductor rather than a metal. We can consider this band structure to be qualitatively reliable in that the anisotropy is consistent with the observed electrical properties of this salt (below). In the meantime, the system still might have a Fermi surface, considering the observed electrical and magnetic properties (below). All in all, considering the EHTB calculation, the observed electrical and magnetic behavior, the system should be located at the borderline of metals and semiconductors, which exhibits a barely metallic nature. Such a feature resembles the β''-salt.[10]

Conducting Properties. Figure 5 shows the temperature and pressure dependence of the resistivity (ρ) of the α-salt, where the current was along the b-axis. It was difficult to measure the ρ under atmospheric pressure, since some jumps in the resistivity were often observed. Thus, Fig. 5 shows only the high-pressure data. From RT to 1.2 K, the temperature and pressure dependences were very small and ρ was nearly constant around 0.04–0.09 Ω cm. In contrast to the β''-salt, a remarkably large pressure-dependence of ρ was not observed in this salt. Considering such a low resistivity and temperature-dependence, this salt should be regarded as being metallic under high pressure, rather than semiconducting, for better consistency with the calculated band structure above and the magnetic behavior discussed below. Under lower pressure, the temperature dependence of ρ exhibited a broad maximum. The maximum moved towards lower temperature, and was gradually suppressed with increasing pressure. At the same

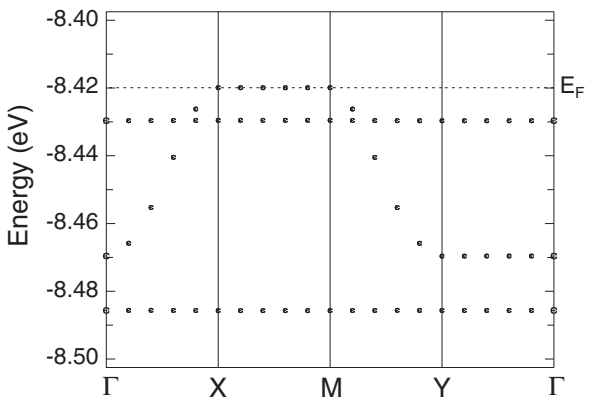

Fig. 4. Tight biding band structure. Top; Fermi surface (broken lines), bottom; band dispersion (dotted curves) with the Fermi level (solid line). Γ, X, M, Y denote the points of (0,0,0), (0,1,0), (0,0.5,0.5), (0,0,1) in the reciprocal space, respectively.

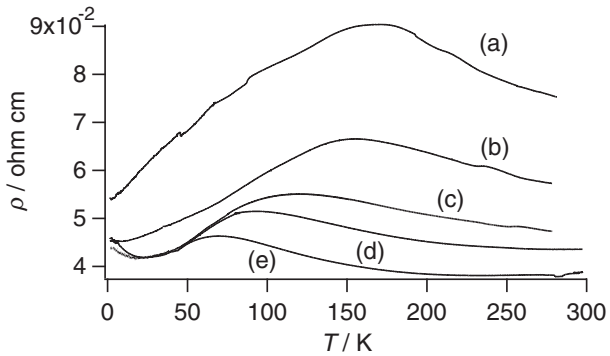

Fig. 5. Pressure and temperature dependences of the resistivity. The measurements were carried out under (a) 2.9 kbar, (b) 5.9 kbar, (c) 8.9 kbar, (d) 11.9 kbar, and (e) 14.8 kbar.

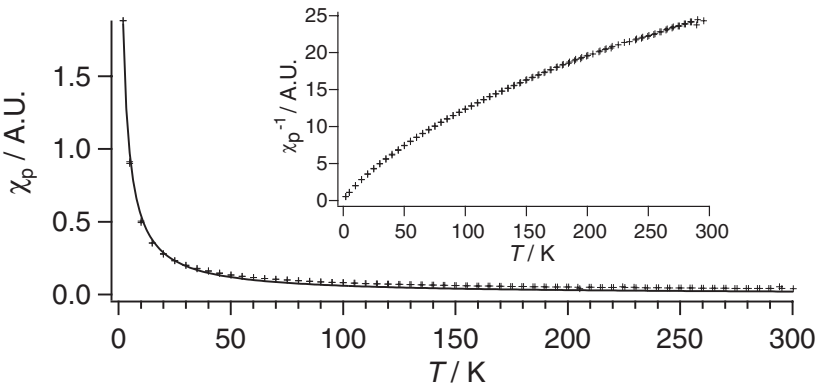

Fig. 6. Temperature dependence of the magnetic susceptibility (χ_p); observed (crosses) and best-fit curve based on the Curie–Weiss law (line). As for the parameters for the curve-fitting, see text. (inset): Temperature dependence of the inverse of χ_p.

time, another rise in the resistivity appeared at a temperature lower than ~30 K. Such a behavior was very sensitive to the crystallographic direction of the measurements; the result was qualitatively different when the current direction was even slightly different. This sensitive anisotropy agrees well with the 1D nature of the electronic structure suggested from the band calculation. Such complicated temperature- and pressure-dependences of the resistivity contrast well with the previously reported molecular metals and semiconductors, many of which exhibit simple temperature- and/or pressure-dependences in their resistivity.[28] A structural study down to 103 K and the magnetic behavior (see below) of the α-salt did not indicate any phase transition in the spin system of $[MnCl_4]^{2-}$ anions, or in the conduction systems of ET cation radicals. Such stability of the 1D electronic structure is unusual, and now remains to be explained. Another interesting feature about this salt concerns how large the effective mass of the conduction electrons is and what phenomena will arise from the mass enhancement. This salt is evidently worthy of further study.

Magnetic Properties. Figure 6 shows the temperature dependence of the magnetic susceptibility (χ_p) of the α-salt. After several independent measurements, the behavior was always approximately reproduced by a Curie–Weiss model with a Weiss temperature of $\theta = -(1.35 \pm 0.07)$ K. The Curie–Weiss-like behavior with a small value of θ is quite similar to that of the β''-salt in a qualitative sense.[10] However, the absolute value of χ_p had a large sample dependence; the Curie constant was $C \approx 3.5$–6.1 emu K mol^{-1}. In the β''-salt, the observed Curie constant C always agreed well with the spin-only value of the Mn(II) atoms. On the contrary, in the α-salt, even if we take only the spins on the $[MnCl_4]^{2-}$ anions ($S = 5/2$) into consideration, these C values correspond to 40–70% of the theoretical value (8.75 emu K per two $[MnCl_4]^{2-}$ anions). Based on the crystal structure of the α-salt mentioned above, the interaction between the local spins on the $[MnCl_4]^{2-}$ anions and the conduction electrons on the ET cations can be expected to be weak. The direct magnetic interaction between the $[MnCl_4]^{2-}$ anions are hardly conceivable because they are too apart from each other (>9 Å). Therefore, no magnetic interactions are expected to result in such a significant decrease in the magnetic moment of the $[MnCl_4]^{2-}$ anions. At least, the magnetic susceptibility strongly suggests that the π-spins on the ET molecules should not be localized down to 2 K. The explanation on the C value requires further study.

In order to obtain information of the conduction electrons at ambient pressure, we measured the temperature-dependent ESR spectra. This salt contains two kinds of unpaired electrons in π- and d-orbitals, respectively. At RT, an apparently single Lorentzian signal was observed (Fig. 7). In the temperature region lower than ~50 K, both contributions from π- and d-electrons appeared as clearly resolved peaks. This behavior can be explained as follows. Firstly, each Mn(II) atom in the $[MnCl_4]^{2-}$ anions should take the d^5 high-spin state, and thus its orbital angular momentum is quenched. Secondly, the g-value of the d-electrons coincides with that of the π-electrons, both being located around 2.00. Thirdly, because there should be few interactions between the d- and the π-electrons, the ESR spectrum is the sum of each contribution at a given temperature. Accordingly, if both of the linewidths decrease upon lowering the temperature, they are well resolved at low temperature, while they are not at around RT. The spectral features, such as anisotropies, absolute values and temperature dependences of the peak-to-peak linewidth (ΔH_{pp}), g-value, and spin susceptibility χ_{spin} greatly resemble those of the structurally related β''-salt.[10] The fine structure due to the spins on the $[MnCl_4]^{2-}$ anions is more clearly observed in the α-salt than

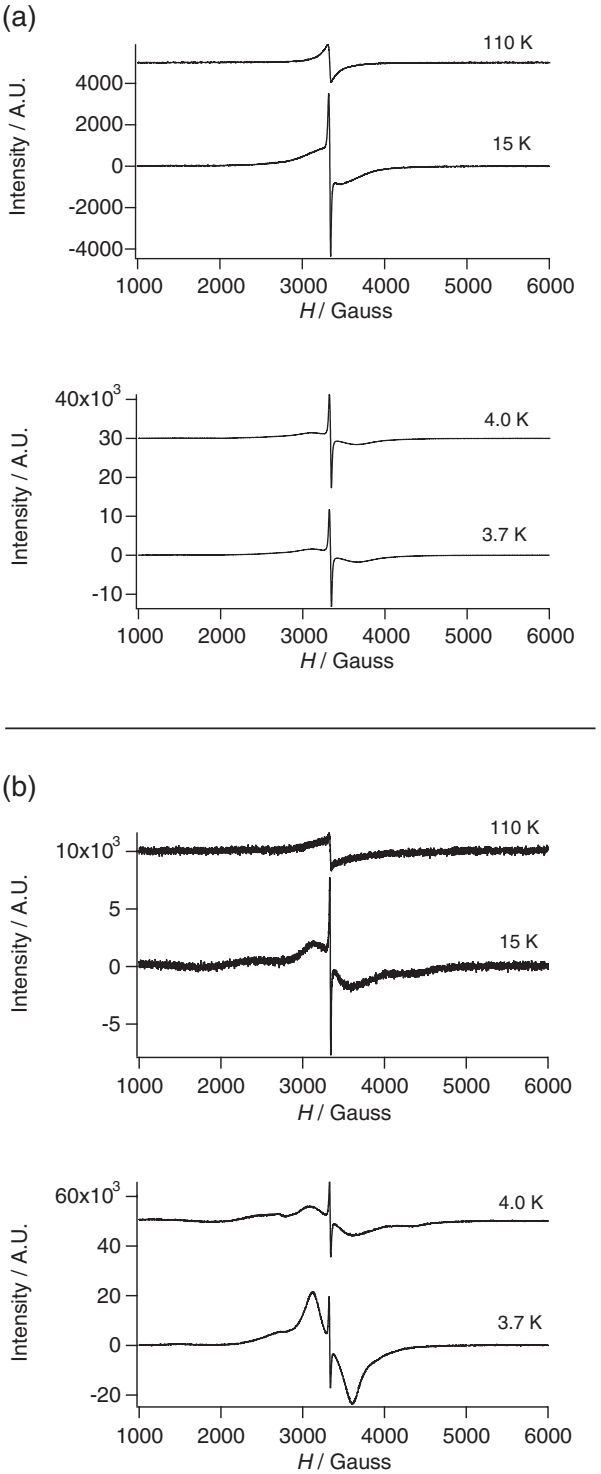

Fig. 7. Temperature dependence of the lineshape of ESR spectra. (a) 0- and (b) 90-spectra.

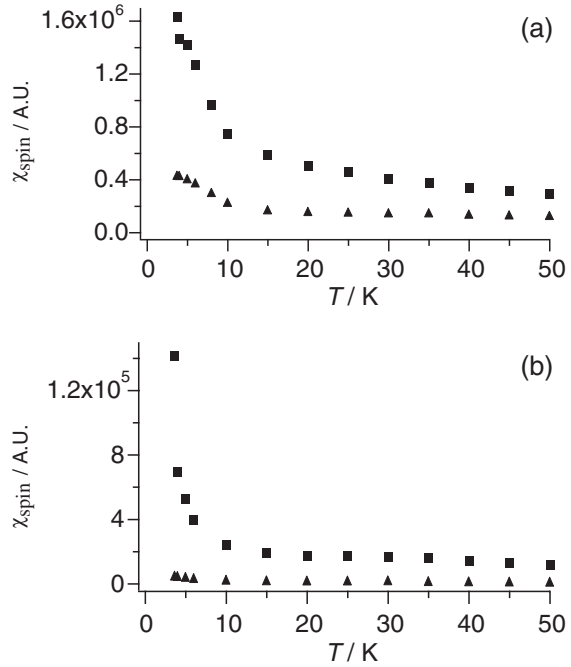

Fig. 8. Temperature dependence of χ_{spin} from ESR spectra. (a) 0- and (b) 90-spectra. Squares and triangles denote d- and π-spins, respectively.

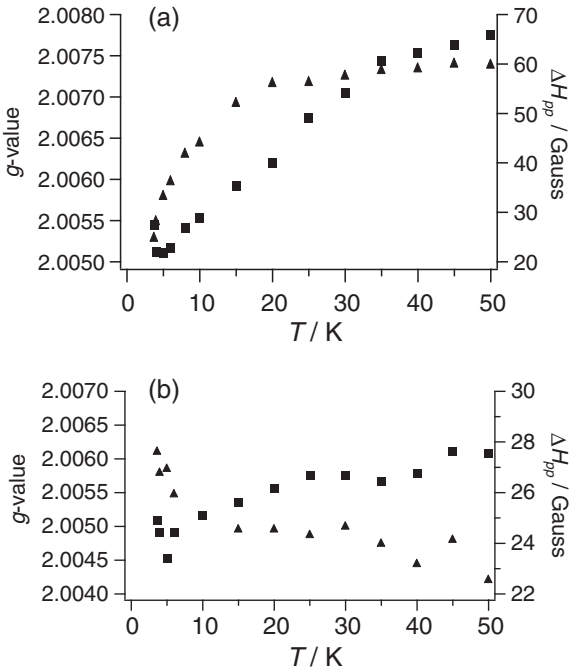

Fig. 9. Temperature dependence of the g-value and the peak-to-peak linewidth ΔH_{pp} of ESR spectra. (a) 0- and (b) 90-spectra. Squares and triangles denote ΔH_{pp} and g-value, respectively.

in the β''- salt.[10] This enables us to separate the two kinds of contributions (π- and d-electrons) from each other in the spectra below ~50 K.

A deconvolution of the spectra was carried out using singly integrated spectra instead of the as-obtained first-derivative ones. In the 0-spectra, we used only two Lorentzian oscillators for the d- and the π-spins, respectively, since the fine structures due to the d-spins on the $[MnCl_4]^{2-}$ anions are not resolved well. In the 90-spectra, we found it best to use four Lorentzian oscillators in total for the d- and the π-spins; a smaller number of oscillators failed to reproduce the peak shoulders that appeared in the integrated spectra, while a larger number failed to converge in the curve-fitting. In this way, we may discuss each behavior of d- and π-spins in a qualitative way at low temperature ($\lesssim$50 K). The temperature dependences of χ_{spin} of π- and d-electrons are shown in Fig. 8. The 90-spectra are considered to manifest the behavior of conduction electrons more clearly than the other. They indicate a temperature-independent behavior of the π-spins with a very small susceptibility, which can be attributed to Pauli paramagnetism. The same spectra show approximately a Curie-type behavior of the d-spins. These results are qualitatively consistent with the magnetic susceptibility measured with a SQUID. Therefore, we can consider that this salt has a metallic electronic structure *under atmospheric pressure*. Combining this information with the results of resistivity measurements, the α-salt is found to exhibit metallic properties down to low temperature under all pressures examined. In the 0-spectra, the separation might not be good in an analysis (deconvolution) of the spectra. The Pauli paramagnetic behavior of the conduction electrons is also qualitatively shown in this result, yet the values of the susceptibilities are very large compared with those of the d-spins; also, an upturn trend appeared at low temperature. This could indicate a localized nature of the π-electrons in any direction other than along the b-axis. Still, we do not discuss the details of the spin susceptibility from the 0-spectra here.

Next, let us examine the temperature dependences of ΔH_{pp} and the g-value of the conduction electrons below ~50 K (Fig. 9). In the 0-spectra, both ΔH_{pp} and the g-value are nearly constant at ~50 K to ~35 K (ΔH_{pp}) or ~50 K to ~20 K (g-value), while they both steeply decrease at lower temperature. In the 90-spectra, the temperature dependences of both ΔH_{pp} and the g-value are small; with lowering temperature, ΔH_{pp} slightly decreases, while the g-value slightly increases. In either case of the 0- and the 90-spectra, a sharp minimum in ΔH_{pp} at 5 K is observed. On the other hand, in the deconvoluted 0- and 90-spectra the d-spins exhibit a very complicated behavior of ΔH_{pp}, the g-values and the spin susceptibilities (not shown). A detailed discussion on these spectra must wait further study.

In summary, we synthesized and characterized a new ET conducting salt, α-$(ET)_7[MnCl_4]_2 \cdot (TCE)_2$. From RT to 2 K (ambient pressure)/1.2 K (high pressure) it exhibits a practically metallic property due to the ET cation radicals. From RT to 2 K it exhibits an approximately Curie–Weiss type magnetic behavior dominated by discrete $[MnCl_4]^{2-}$ anions. An EHTB band calculation suggests that it should have a narrow HOMO band. Although such an electronic structure is well known to be unstable, and subject to cause a metal-to-insulator transition or localization at low temperature, the title salt does not exhibit any insulating behavior down to low temperature. The interaction between the conduction and localized electrons in this salt is negligibly small. Some details of observed electrical and magnetic properties remain to be clarified by further study.

We thank Profs. T. Nakamura, T. Akutagawa at RIES, Hokkaido University, and Dr. T. Hasegawa at AIST for helping us in the electrical measurements and discussion. We also thank Prof. T. Mori at Tokyo Institute for Technology and H. Mori at ISSP, The University of Tokyo for helping us in the discussion of the crystal and band structures. We are grateful to Dr. M. Wakesima and Prof. Y. Hinatsu at Hokkaido University for helping us in the susceptibility measurement with SQUID at their laboratory.

References

1 P. Day, M. Kurmoo, T. Mallah, I. R. Marsden, R. H. Friend, F. L. Pratt, W. Hayes, D. Chasseau, J. Gaultier, G. Bravic, and L. Ducasse, *J. Am. Chem. Soc.*, **114**, 10722 (1992).

2 A. Kobayashi, T. Udagawa, H. Tomita, T. Naito, and H. Kobayashi, *Chem. Lett.*, **1993**, 2179.

3 M. Kurmoo, A. W. Graham, P. Day, S. J. Coles, M. B. Hursthouse, J. L. Caulfield, J. Singleton, F. L. Pratt, W. Hayes, and L. Ducasse, *J. Am. Chem. Soc.*, **117**, 12209 (1995).

4 H. Kobayashi, H. Tomita, T. Naito, A. Kobayashi, F. Sakai, T. Watanabe, and P. Cassoux, *J. Am. Chem. Soc.*, **118**, 368 (1996).

5 H. Kobayashi, A. Kobayashi, and P. Cassoux, *Chem. Soc. Rev.*, **29**, 325 (2000).

6 E. Coronado, J. R. Galán-Mascarós, C. J. Gómez-García, and V. Laukhin, *Nature*, **408**, 447 (2000).

7 S. Uji, H. Shinagawa, T. Terashima, T. Yakabe, Y. Terai, M. Tokumoto, A. Kobayashi, H. Tanaka, and H. Kobayashi, *Nature*, **410**, 908 (2001).

8 T. Mori and H. Inokuchi, *Bull. Chem. Soc. Jpn.*, **61**, 591 (1988).

9 M. Lequan, R. M. Lequan, G. Maceno, and P. Delhaes, *J. Chem. Soc., Chem. Commun.*, **1988**, 174.

10 T. Naito, T. Inabe, K. Takeda, K. Awaga, T. Akutagawa, T. Hasegawa, T. Nakamura, T. Kakiuchi, H. Sawa, T. Yamamoto, and H. Tajima, *J. Mater. Chem.*, **11**, 2221 (2001).

11 H. Miyasaka, Y. Yoshino, T. Ishii, R. Kanehama, T. Manabe, M. Yamashita, H. Nishikawa, I. Ikemoto, H. Kishida, H. Matsuzaki, and H. Okamoto, *J. Solid State Chem.*, **168**, 418 (2002).

12 T. Naito and T. Inabe, *J. Solid State Chem.*, **176**, 243 (2003).

13 R. Kanehama, H. Miyasaka, K. Sugiura, M. Yamashita, H. Itou, S. Kuroda, H. Kishida, and H. Okamoto, *Synth. Met.*, **135–136**, 633 (2003).

14 T. Lis, *Acta Crystallogr., Sect. B*, **36**, 2042 (1980).

15 R. Sessoli, H.-L. Tsai, A. R. Schake, S. Wang, J. B. Vincent, K. Folting, D. Gatteschi, G. Christou, and D. N. Hendrickson, *J. Am. Chem. Soc.*, **115**, 1804 (1993).

16 H. J. Eppley, H.-L. Tsai, N. de Vries, K. Folting, G. Christou, and D. N. Hendrickson, *J. Am. Chem. Soc.*, **117**, 301 (1995).

17 A. Altmare, M. C. Burla, M. Camalli, M. Cascarano, C. Giacovazzo, A. Guagliardi, and G. Polidori, *J. Appl. Crystallogr.*, **27**, 435 (1994).

18 D. T. Cromer and J. T. Waber, "International Tables for X-ray Crystallography," The Kynoch Press, Birmingham, England (1974), Vol. IV, Table 2.2 A.

19 D. C. Creaghand and J. H. Hubbell, "International Tables for X-ray Crystallography, Vol. C," ed by A. J. C. Wilson, Kluwer Academic Publishers, Boston (1992), pp. 200–206, Table 4.2.4.3.

20 "teXsan; Crystal Structure Analysis Package," Molecular Structure Corporation, 3200 Research Forest Drive, The Woodlands, TX 77381 (1985 and 1992).

21 L. J. Farrugia, *J. Appl. Crystallogr.*, **30**, 565 (1997), the program is available from the following URL, http://www.chem.gla.ac.uk/~louis/ortep3/.

22 J. Ren, W. Liang, and M. H. Whangbo, "Crystal and Electronic Structure Analysis Using CAESAR," PrimeColor Software, Inc. (1998), (this book can be downloaded free of charge from the website: http://www.PrimeC.com/).

23 J. Ammeter, H. B. Bürgi, J. Thibeault, and R. Hoffmann, *J. Am. Chem. Soc.*, **100**, 3686 (1978).

24 T. Mori, P. Wang, K. Imaeda, T. Enoki, H. Inokuchi, F. Sakai, and G. Saito, *Synth. Met.*, **27**, A451 (1988).

25 a) K. Bender, I. Hennig, D. Schweitzer, K. Dietz, H. Endres, and H. J. Keller, *Mol. Cryst. Liq. Cryst. Sci. Technol.*, **108**, 359 (1984). b) T. Mori, H. Mori, and S. Tanaka, *Bull. Chem. Soc. Jpn.*, **72**, 179 (1999).

26 K. A. Abboud, M. B. Clevenger, G. F. de Oliveira, and D. R. Talham, *J. Chem. Soc., Chem. Commun.*, **1993**, 1560.

27 P. Guinneau, C. J. Kepert, D. Chasseau, M. R. Truter, and P. Day, *Synth. Met.*, **86**, 1973 (1997).

28 a) *Synth. Met.*, **133–134** (2003), "Special Issue: ISCOM 2001," ed by G. Saito, S. Kagoshima, K. Kanoda, H. Aoki, T. Mori, Y. Misaki, and H. Yamochi, Elsevier, Shannon (2003). b) J. Wosnitza, "Fermi Surfaces of Low-Dimensional Organic Metals and Superconductors," Springer-Verlag, New York (1996). c) J. M. Williams, J. R. Ferraro, R. J. Thorn, K. D. Carlson, U. Geiser, H. H. Wang, A. M. Kini, and M.-H. Whangbo, "The Physics and Chemistry of Organic Superconductors (Including Fullerenes)," Prentice Hall, New Jersey (1992). d) G. Saito and S. Kagoshima, "The Physics and Chemistry of Organic Superconductors," Springer-Verlag, Berlin (1990). e) T. Ishiguro and K. Yamaji, "Organic Superconductors," Springer-Verlag, Berlin (1989). f) J. M. Williams, H. H. Wang, T. J. Emge, U. Geiser, M. A. Beno, P. C. W. Leung, K. D. Carlson, R. J. Thorn, A. J. Schultz, and M.-H. Whangbo, *Prog. Inorg. Chem.*, **35**, 51 (1987). g) D. Jérome and H. J. Schulz, *Adv. Phys.*, **31**, 299 (1982).